https://doi.org/10.5194/egusphere-2022-835
Preprint. Discussion started: 5 October 2022

Modeling of non-structural carbohydrate dynamics by the spatially explicitly individual-based dynamic global vegetation model SEIB-DGVM (SEIB-DGVM-NSC ver1.0)

Hideki Ninomiya[1], Tomomichi Kato[2], Lea Végh[2], and Lan Wu[3]

[1]Graduate School of Global Food Resources, Hokkaido University, Sapporo, Hokkaido 060-0809, Hokkaido, Japan
[2]Research Faculty of Agriculture, Hokkaido University, Sapporo, Hokkaido 060-8589, Japan
[3]College of Ecology and Environment, Hainan University, Hainan, China

Correspondence: Tomomichi Kato (tkato@cen.agr.hokudai.ac.jp)
Tel & Fax: +81 11 706 4942

Abstract. Forest dynamics need to be considered when estimating the global carbon budget. The alteration of forest structure and function under a changing climate and expanding human activity could lead to a reduction of forest canopy cover and a spread of lower-biomass ecosystems in warm and dry regions. Non-structural carbohydrate (NSC) acts as a storage buffer between carbon supplied by assimilation and carbon consumed by, inter alia, respiration, reproduction, and pests. Estimation of NSC concentrations in a tree is very important for accurate projection of future forest dynamics. We developed a new NSC module for incorporation into a spatially explicit, individual-based, dynamic global vegetation model (SEIB-DGVM) to validate the simulated NSC dynamics with observations. NSC pools were simulated in three plant organs: leaves, trunk, and roots. The seasonal dynamics of the NSCs varied among plant species, and the sizes of the NSC pools inferred from observations differed between the boreal, temperate, and tropical climates. The NSC models were therefore validated for each of the three climatic regions at both point and global scales to assess the performance of the models. The modeled NSCs showed good agreement in seasonality with the observed NSCs at four sites—Canada (boreal), Austria and Switzerland (temperate), and Panama (tropical)—and in mean values for three climate zones derived from the global NSC dataset. The SEIB-DGVM-NSCv1.0 is expected to enable simulation of biome shifts caused by the changes of NSC dynamics worldwide. These dynamics will contribute to changes of not only the global carbon cycle but also of forest structure and demography at a global scale.

https://doi.org/10.5194/egusphere-2022-835
Preprint. Discussion started: 5 October 2022

1 Introduction

Permanent shifts in forest vegetation dynamics have already been observed and are expected to accelerate under future changes of climate globally (McDowell et al., 2020). Forest dynamics are changing due to anthropogenic drivers, such as rising temperatures and CO_2 partial pressures, and are affected by transient disturbances such as wildfires, droughts, biotic attacks, and land-use changes. The dependence of tree recruitment and growth on spatial and temporal drivers could lead to an increase of tree mortality rates in warm and dry regions (Stevens-Rumann et al., 2018; Xu et al., 2017). These changes will cause forests to become shorter and younger. The result will be a net reduction of forest canopy cover and a shift toward low-biomass ecosystems. Furthermore, higher tree mortality will have a negative impact on global ecosystem: lower biological diversity, a decrease of wild animal habitat, altered hydrological and carbon cycles, and increased vulnerability to sudden invasions by exotic species (Adams et al., 2013). Understanding the drivers of vegetation dynamics requires accurately simulating the effect of climate change on global terrestrial biogeochemistry.

To increase their chance of survival, trees control their carbon resources and strategically allocate them to growth, respiration, storage, reproduction, and defense (Hoch et al., 2003; Hartmann et al., 2018). When the atmospheric partial pressure of CO_2 increases, trees can allocate surplus carbon to either growth or carbon storage (Hoch et al., 2003; Huang et al., 2020). Changes in tree carbon allocation patterns have been shown to exert large effects on constituents of the terrestrial carbon cycle (Klein and Hoch, 2015). Clarification of the importance of carbon allocation has revealed that non-structural carbohydrates (NSCs) draw much from the other carbon resources because they are the most significant carbon compounds involved in the life processes of trees (He et al., 2020).

The NSC is comprised of starch and sugars, which are mobilized mainly for growth and metabolism when little recently assimilated carbon is available (Gough et al., 2010; Richardson et al., 2013; Chuste et al., 2020; Herrera-Ramírez et al., 2020). During photosynthesis, freshly assimilated carbon is transported as triose phosphate from the chloroplast to the cytosol, where sucrose is synthesized from it. Some of the sucrose is then changed into starch in the chloroplast, and the starch is consumed to maintain growth and metabolism at times when recently assimilated carbon is not available to the plants (Dietze et al., 2014). Plants that seasonally shed leaves need to rely on stored carbon for maintenance during the leafless season. NSCs play an important role as substrates for the synthesis of compounds in plants and as energy sources for metabolic activities (Hartmann et al., 2018). Moreover, NSCs include key compounds that are used to buffer physiological stress when energy from photosynthesis does not satisfy metabolic demands (Gough et al., 2010; Sala et al., 2012) because carbohydrates such as starch can be easily

https://doi.org/10.5194/egusphere-2022-835
Preprint. Discussion started: 5 October 2022

mobilized and reallocated (Hartmann et al., 2018).

In long-lived plants, the ability to store carbon is a key to survival at times when photosynthetic rates are low because of shade, drought, and disturbance (Martínez-Vilalta et al., 2016). As a result, the amount of NSC depends on the balance between the supply and demand of assimilated carbon and accounts for a large fraction of the annual carbon budget of plants (Richardson et al., 2013). When carbon allocation patterns favor storage over growth, tree growth is limited (Wang et al., 2021). Hence, the dynamics of stored carbon pools can be considered an indicator of the carbon balance of the plant.

Because the frequency, duration, and severity of droughts are expected to increase globally, the damage to plants through rising temperatures, water vapor pressure deficiency, and associated water loss will also increase (IPCC, 2014; Sevanto and Dickman, 2015). Trees are killed directly by drought or indirectly by associated increases of insect or pathogen attacks. Indirect effects that cause tree mortalities include girdling of the phloem and xylem by bark beetles and defoliation events that delay recovery of trees. The frequency and severity of this indirect biotic disturbance from insects and insect–pathogen complexes have been increasing (McDowell et al., 2020; Seidl et al., 2017). According to multiple observational and experimental studies, the resulting imbalance between NSC demand and supply leads to carbon starvation, which is one of the mechanisms that contribute to drought-induced mortality (McDowell, 2011).

The decline of stomatal conductance during a drought reduces photosynthetic carbon assimilation and thus decreases the amount of NSC (McDowell et al., 2008; Adams et al., 2017). Although an imbalance of the NSC pool could mechanistically trigger plant mortality, few ecological models predict tree mortality resulting from the role of NSC associated with climate change (Adams et al., 2013; McDowell, 2011). Simulations of the NSC dynamics of plants will elucidate the effects of different drivers on forested ecosystems (Gough et al., 2010).

Dynamic global vegetation models (DGVMs) are often used to represent vegetation dynamics as well as biogeochemical cycles and to simulate the transition of the vegetation structure in response to climatic changes via modeling of competition and disturbance (Hickler et al., 2004; Krinner et al., 2005; Braakhekke et al., 2019). In DGVMs, plant species are classified into plant functional types (PFTs) based on their eco-physiological traits. However, most DGVMs oversimplify individual plant competition by using average values of traits for each PFT (Smith et al., 2001). Most of such models miss the effects of local competition for light, which must be considered when modeling gap population dynamics among individual trees (Sato et al., 2007).

In contrast, the Spatially Explicit, Individual-Based, Dynamic Global Vegetation Model (SEIB-DGVM; Sato et al., 2007) can simulate the growth of individual trees on numerous replicate patches and enable observation of how single, large trees can influence nearby trees. Plants in different patches do not interact with each other in terms of physical resources such as

https://doi.org/10.5194/egusphere-2022-835
Preprint. Discussion started: 5 October 2022

light and water. In each patch, the growth, competitive interactions, and mortality of each tree are calculated based on environmental conditions. Transient changes in vegetation distribution and dynamics can therefore be examined (Sato et al., 2007).

SEIB-DGVM has been used to simulate a transient change in the distribution and function of vegetation on the African continent in conjunction with the ranges of dispersal of trees and to address factors that had a strong impact on the transient change (Sato and Ise, 2012). Use of the SEIB-DGVM has enabled reconstruction of the geographical distributions of plant productivity and thermo-hydrology based on observations in eastern Siberia and partial representation of the effect of topography on the abundance of trees in larch forests (Sato et al., 2020). The SEIB-DGVM was coupled with a flagship Earth system model (MIROC-ESM; Watanabe et al., 2011). Because the amount of stored NSC depends on the size of individual trees and because the SEIB-DGVM can simulate individual trees, we chose the SEIB-DGVM to estimate the NSC dynamics of plants.

The objectives of the research were to 1) incorporate a module to simulate NSC dynamics in the SEIB-DGVM and 2) validate the simulated NSC dynamics with observational data at both point and global scales. We therefore created a new function in the SEIB-DGVM to represent the NSC dynamics of individual trees. How NSC is produced, stored, and distributed among different plant organs under environmental stress is poorly understood (Jones et al., 2019; Rademacher et al., 2021; Wang et al., 2021). Our enhanced model improves the physiological simulation of the leaf life cycle and enhances understanding of how NSC affects the distribution of vegetation, gross primary production (GPP), net primary production (NPP), and carbon stocks as well as tree dynamics (age, height, and trunk diameter) at global scales in the future. By adjusting the NSC accumulation rates of individual trees and the threshold of NSC-induced mortality during drought, the model can simulate the timing, location, and percentage of trees that die in response to moderate drought. Furthermore, the model can increase our understanding of the role of carbon reserves.

2 Model

2.1 Spatially Explicit Individual-Based Dynamic Global Vegetation Model (SEIB-DGVM)

The SEIB-DGVM (v3.02; http://seib-dgvm.com/data/seib_code302.zip; Sato et al., 2016) is a carbon budget model that simulates the establishment of individual trees, competition between trees, and the death of individual trees according to input climate data. The default settings follow the structure of a three-dimensional virtual forest on a 30 m × 30 m stand of trees with 1 m × 1 m simulation grid cells. In each grid cell, a tree belonging to one of 14 woody plant functional types

https://doi.org/10.5194/egusphere-2022-835
Preprint. Discussion started: 5 October 2022

(PFTs) is assigned if conditions allow in addition to one of 2 grass PFTs. All physical and physiological processes are calculated at daily time steps, trunk growth is estimated monthly, and vegetation dynamics and disturbance are assessed annually. Because of the lack of field observations at the time the model was developed, there is no mechanism to control the carbon stock in leaves and roots in the original SEIB-DGVM, and only the carbon stock in trunks is simulated after adjusting the available organic matter for reproduction and respiration. The original SEIB-DGVM therefore cannot represent carbon starvation effectively without accounting for the carbon stock in leaves and roots, even though the carbon stock of the trunk depends on the leaf mass from the previous day.

2.2 NSC components

2.2.1 NSC pool

The new NSC pools are separated into three organs of an individual tree: leaves, trunk, and roots. The original SEIB-DGVM simply allocates the surplus carbon that remains after respiration for the growth of roots and then, if more than 30 days have passed since foliation, for the growth of leaves and the trunk. In this study, the carbon newly assimilated via photosynthesis goes into three NSC pools. The NSC pools can be later mobilized for growth and respiration as follows (Fig. 1).

$$\Delta NSC_t = NPP_t = \Delta NSC_{trunk,t} + \Delta NSC_{leaf,t} + \Delta NSC_{root,t}, \quad (1)$$

when $NSC_{trunk,\,t-1} < NSC_{trunk,\,max(t)}$, $NSC_{leaf,\,t-1} < NSC_{leaf,\,max(t)}$, and $NSC_{root,\,t-1} < NSC_{root,\,max(t)}$,

$$\begin{cases} \text{parent } NSC_{trunk,t} = \min\left(NSC_{trunk,max\,(t)}, \Delta NSC_t\right), \\ NSC_{leaf,t} = \min\left(NSC_{leaf,max\,(t)}, \Delta NSC_t - NSC_{trunk,t}\right), \\ NSC_{root,t} = \min\left(NSC_{root,max(t)}, \Delta NSC_t - NSC_{trunk,t} - NSC_{leaf,t}\right), \end{cases} \quad (2)$$

when $NSC_{trunk,\,t-1} < NSC_{trunk,\,max(t)}$, $NSC_{leaf,\,t-1} < NSC_{leaf,\,max(t)}$, and $NSC_{root,\,t-1} > NSC_{root,\,max(t)}$

$$\begin{cases} NSC_{trunk,t} = \min\left(NSC_{trunk,max(t)}, \Delta NSC_t\right), \\ NSC_{leaf,t} = \min\left(NSC_{leaf,max(t)}, \Delta NSC_t - NSC_{trunk,t}\right), \\ NSC_{root,t} = NSC_{root,max(t)} \end{cases} \quad (3)$$

when $NSC_{trunk,\,t-1} < NSC_{trunk,\,max(t)}$, $NSC_{leaf,\,t-1} > NSC_{leaf,\,max(t)}$, and $NSC_{root,\,t-1} < NSC_{root,\,max(t)}$,

https://doi.org/10.5194/egusphere-2022-835
Preprint. Discussion started: 5 October 2022

$$\begin{cases} NSC_{trunk,t} = \min\left(NSC_{trunk,max(t)}, \Delta NSC_t\right), \\ NSC_{leaf,t} = NSC_{leaf,max\,(t)}, \\ NSC_{root,t} = \min\left(NSC_{root,max(t)}, \Delta NSC_t - NSC_{trunk,t} - NSC_{leaf,t}\right), \end{cases} \quad (4)$$

when $NSC_{trunk,\,t-1} < NSC_{trunk,\,max(t)}$, $NSC_{leaf,\,t-1} > NSC_{leaf,\,max(t)}$, and $NSC_{root,\,t-1} > NSC_{root,\,max(t)}$,

$$\begin{cases} \text{parent } NSC_{trunk,t} = \min\left(NSC_{trunk,max(t)}, \Delta NSC_t\right), \\ NSC_{leaf,t} = NSC_{leaf,max\,(t)}, \\ NSC_{root,t} = NSC_{root,max\,(t)}, \end{cases} \quad (5)$$

when $NSC_{trunk,\,t-1} > NSC_{t,\,max(t)}$, $NSC_{leaf,\,t-1} < NSC_{leaf,\,max(t)}$, and $NSC_{root,\,t-1} < NSC_{root,\,max(t)}$,

$$\begin{cases} NSC_{trunk,t} = NSC_{t,max(t)} \\ NSC_{leaf,t} = \min\left(NSC_{leaf,max\,(t)}, \Delta NSC_t\right), \\ NSC_{root,t} = \min\left(NSC_{root,max(t)}, \Delta NSC_t - NSC_{trunk,t} - NSC_{leaf,t}\right), \end{cases} \quad (6)$$

when $NSC_{trunk,\,t-1} > NSC_{t,\,max(t)}$, $NSC_{leaf,\,t-1} < NSC_{leaf,\,max(t)}$, and $NSC_{root,\,t-1} > NSC_{root,\,max(t)}$,

$$\begin{cases} NSC_{trunk,t} = NSC_{t,max(t)}, \\ NSC_{leaf,t} = \min\left(NSC_{leaf,max\,(t)}, \Delta NSC_t\right), \\ NSC_{root,t} = NSC_{root,max(t)}, \end{cases} \quad (7)$$

when $NSC_{trunk,\,t-1} > NSC_{t,\,max(t)}$, $NSC_{leaf,\,t-1} > NSC_{leaf,\,max(t)}$, and $NSC_{root,\,t-1} < NSC_{root,\,max(t)}$,

$$\begin{cases} NSC_{trunk,t} = NSC_{t,max(t)}, \\ NSC_{leaf,t} = NSC_{leaf,max(t)}, \\ NSC_{root,t} = \min\left(NSC_{root,max\,(t)}, \Delta NSC_t\right), \end{cases} \quad (8)$$

when $NSC_{trunk,\,t-1} > NSC_{t,\,max(t)}$, $NSC_{leaf,\,t-1} > NSC_{leaf,\,max(t)}$, and $NSC_{root,\,t-1} > NSC_{root,\,max(t)}$,

$$\begin{cases} NSC_{trunk,t} = NSC_{t,max(t)}, \\ NSC_{leaf,t} = NSC_{leaf,max(t)}, \\ NSC_{root,t} = NSC_{root,max\,(t)}, \end{cases} \quad (9)$$

where t is the calculation day, t-1 is the previous day, NSC_{organ} is the amount of NSC in each organ, and $NSC_{organ,\,max(t)}$ is the maximum amount of NSC in each organ on day t.

https://doi.org/10.5194/egusphere-2022-835
Preprint. Discussion started: 5 October 2022

First, the surplus carbon that remains after respiration is assigned to the NSC trunk pool using Eq. (1). As long as the trunk biomass increases relative to that on the previous day, the overflowing carbon moves primarily into NSC_{leaf}, secondarily into NSC_{root}, and finally into the growth of leaves, the trunk, and roots. The sum of the NSCs in the leaves, trunk, and roots (the total NSC) is maximized for each climate region (Table 1). If the total NSC exceeds this upper limit, the surplus is directly consumed for the growth of each organ.

Table 1. Maximum volume of NSC pool

	Maximum of NSC pool	
Boreal	10% of total biomass	Martínez-Vilalta et al. (2016)
Temperate	5% of total biomass	Hoch et al. (2003)
Tropical	9% of total biomass	Würth et al. (2005)

The NSC pools of the organs displays unique seasonality for each climatic zone. The NSC seasonality of each organ varies among tree species mainly because the climate and surrounding environment influence the capacity and utilization of NSCs in plants. To take into consideration the fact that field observations of NSC covered whole seasons and that various plant species were scarce, we classify NSC seasonality into three types: tropical, temperate, and boreal. Observations from temperate forests showed that the NSC seasonal cycles were similar among the organs and peaked around late spring–summer, although the NSC_{organ} differed in size (Hoch et al., 2003; Richardson et al., 2013; Woodruff and Meinzer, 2011; Gruber et al., 2012). In contrast, the NSC concentrations in the leaves of boreal trees peak in June (Sveinbjörnsson et al., 2010), and NSCs in the fine roots increase until summer and then decline toward mid-summer and fall because of the initiation of root growth (Landhäusser and Lieffers, 2003). All 14 woody PFTs of the SEIB-DGVM are sorted into one of three NSC types, and carbon assimilated via photosynthesis was allocated to the NSC pool of each organ in temperate and boreal PFTs as follows.

$$NSC_{organ,\,max} = (a + b \times \text{daily GPP}) \times \text{Biomass}, \quad (10)$$

where the organ is either a leaf, trunk, or root, a is the minimum value, and b is the seasonality parameter.

Tropical species have a different NSC seasonality from temperate and boreal species. The NSC of leaves display a concave upward seasonal pattern that reaches its minimum in late spring–early summer (Würth et al., 2005), which is a dry season when leaf production and flowering deplete NSC pools. Singh and Srivastava (1986) have observed that the NSC of roots is at a minimum level from July to September because the NSC pool is drained to enable survival of the

https://doi.org/10.5194/egusphere-2022-835
Preprint. Discussion started: 5 October 2022

rainy season during that period. The amount of NSCs then increases toward winter, when the fine root biomass declines. Hence, Eq. (10), which is used for temperate and boreal forests, is inadequate for simulation of tropical forests because the NSC depends less on the seasonality of photosynthesis in the tropics. The size of the NSC pool of tropical species therefore accumulates as follows.

$$NSC_{organ,\,max} = (a + b) \times \text{Biomass}, \quad (11)$$

where the organ is either the leaf, trunk, or root, a is the minimum value, and b is the seasonality parameter.

2.2.2 NSC expenditure

2.2.2.1 Respiration

Normally, photosynthetically assimilated carbon is used for maintenance respiration without entering the carbon storage system. When the assimilated carbon is inadequate for maintenance respiration, the NSC compensates for the shortage. The NSC loss is allocated to each organ as follows.

$$NSC_{leaf,\,t} = NSC_{leaf,\,t-1} - R_{a,\,t-1} \times c_{leaf} \quad (12)$$

$$NSC_{trunk,\,t} = NSC_{trunk,\,t-1} - R_{a,\,t-1} \times c_{trunk} \quad (13)$$

$$NSC_{root,\,t} = NSC_{root,\,t-1} - R_{a,\,t-1} \times c_{root}, \quad (14)$$

where autotrophic respiration (R_a) is the difference between assimilated carbon and maintenance respiration and c is the allocation factor for NSC utilization ($c_{leaf} + c_{trunk} + c_{root} = 1$). If the total NSC equals the carbon shortfall, the NSC of all organs becomes zero. The allocation factors of NSC utilization depend on the climatic region (Table 2). If an NSC_{organ} is inadequate to provide the allocated share of R_a, the other organs will supply the difference: the NSC_{leaf} is supplemented first from the NSC_{trunk}, and if that is not enough, from the NSC_{root}. Similarly, if any of the other NSC_{organ} pools is unable to cover local shortages, the NSC pools of the remaining organs will balance the supply and demand.

Table 2. Allocation ratio (c) of NSC to organs

Organ	Boreal	Temperate	Tropical
Leaf	0.20	0.05	0.01

https://doi.org/10.5194/egusphere-2022-835
Preprint. Discussion started: 5 October 2022

Trunk	0.60	0.90	0.98
Root	0.20	0.05	0.01

2.2.2.2 Dormancy

In SEIB-DGVM, deciduous PFTs have dormant and growth phases. When the PFTs enter the bud flush phase, the NSC will be consumed. The NSC is allocated at the rates shown in Table 2.

2.2.2.3 Turnover

Part of the NSC pools of leaves and roots is transformed into litter at the same fractional rates as in the turnover of general carbon pools for leaves and roots. This turnover is calculated at daily steps, regardless of the phenology phase.

2.2.2.4 Establishment

The establishment process is performed on the last day of each simulation year in the SEIB-DGVM. The characteristics of the PFT are determined by five bioclimatic parameters: (1) the maximum temperature in the coldest month; (2) the maximum growing-degree day; (3) the minimum growing-degree day; (4) the minimum photosynthetically active radiation; and (5) the duration of drought. All new trees, independent of their PFT, start with a sapwood diameter of 0.01 m and heartwood diameter of 0.00 m. Initially, these new trees have no leaves or fine roots. Their carbon cycle is therefore maintained by initial values of 250 g dry matter (DM) of assimilated carbon and 250 g DM of NSC (NSC_{leaf} = 10 g, NSC_{trunk} = 190 g, and NSC_{root} = 50 g) from the litter pool.

2.3 Validation of NSC for local and global simulations

Observational NSC data for model validation were derived from Martínez-Vilalta et al. (2016), who reviewed 296 papers and summarized NSC dynamics in forests. Their data include total NSCs in leaves, trunks, and roots of mature terrestrial plants from observations lasting at least four months. These data were used for both the local-scale and the global-scale model validations mixed with other sources described below.

2.3.1 Validation at field points

https://doi.org/10.5194/egusphere-2022-835
Preprint. Discussion started: 5 October 2022

2.3.1.1 Site descriptions

For the point-scale validation, we selected locations where NSC data were available for all organs. Four countries satisfied these criteria and were used to validate the simulated NSC content in the plant organs: Canada (boreal), Austria and Switzerland (temperate), and Panama (tropical). At each site, the seasonality of the NSC was measured for at least four months. We used local climate data from meteorological stations gap-filled by corrected gridded climate reanalysis data as the input at these sites. We ran the NSC module including the SEIB-DGVM with the location and climate provided and compared the model output with the observation data.

The boreal site was located near Alder Flats, Alberta, Canada (52°58'N, 114°59'W) in 2000. The site was dominated by boreal winter deciduous plants such as *Populus tremuloides* (Landhäusser and Lieffers, 2003). One of the temperate sites was located in the timberline ecotone at Mt. Patscherkofel to the south of Innsbruck, Austria (47°13′N, 11°27′E) in 2008 (Gruber et al., 2011). Temperate conifer species such as *Pinus cembra* were the dominating tree species. The mean annual air temperature is 2.5°C, with a maximum of 26.0°C in summer and a minimum of −28.0°C in winter. The mean annual precipitation is 995 mm. The other temperate site was at the Mont Noble, Canton Valais, Swiss Central Alps (46°12′N, 7°30′E) and was dominated by temperate conifers (*P. cembra* L.; Hoch et al., 2003) in 2000. The mean annual precipitation is 630 mm. The growing season lasts from early May to early October, and the mean temperature during that time is 6.5°C. The tropical site was located at the Parque Natural Metropolitano near Panama City, the Republic of Panama in 1996 (85°8′N, 79°34′W; Würth et al., 2005). The site has mixed cover with 17 dominant species, including *Cecropia longipes* and *Anacardium excelsum*. The mean annual temperature is 27°C, and the mean annual precipitation was 2,120 mm during 1993–1995 measured at 1.6 km from the site with a canopy crane (data from the Panama Canal Commission, meteorological and hydrological branch).

2.3.1.2 Input climate data

The SEIB-DGVM requires ten climatic variables as environmental drivers: air temperature, soil temperature at a depth of 50 cm (soil layer 1), soil temperature at a depth of 100 cm (soil layer 2), soil temperature at a depth of 150 cm (soil layer 3), precipitation, shortwave radiation, longwave radiation, wind velocity, specific humidity, and diurnal range of air temperature. The input climate data were prepared by harmonizing a global reanalysis gridded climate dataset, the WATCH Forcing Data ERA-Interim (WFDEI, 0.5 × 0.5 degrees, 1979–2016, Weedon et al., 2018), and the climate generated by the SEIB generator (Tei et al., 2017), which is the monthly observation-based climatic datasets produced by Climatic Research Unit (CRU

https://doi.org/10.5194/egusphere-2022-835
Preprint. Discussion started: 5 October 2022

TS4.00, 0.5 × 0.5 degrees, 1901-2015, Harris et al., 2014) supplemented with the National Centers for Environmental Prediction/National Center for Atmospheric Research (NCEP/NCAR) daily climate datasets (Kalnay et al., 1996) for 1950, with local climatology recorded at meteorological stations near the sites. Local climatology in Panama is measured at the Parque Natural Metropolitano Canopy Crane meteorological station (1995–2019). The climatology in Austria (1979–2008) and Switzerland (1979–2000) was derived from the closest meteorological station to the field site under the European Climate Assessment (Klein et al., 2002, https://www.ecad.eu). WFDEI data were used for the climatology in Canada, except for precipitation data, which are measured in the Meteorological Service of Canada (1979–1984, https://climate.weather.gc.ca/historical_data/search_historic_data_e.html).

The reanalysis of daily WFDEI and SEIB climate data included daily records, which were corrected by regression models to local climate data. For temperature, humidity, and shortwave radiation values, local climatology were used directly and the daily WFDEI data supplemented by simple linear regression. Precipitation data and wind speeds were first adjusted to monthly and then annual averages and then scaled as a correction. WFDEI precipitation data were scaled after adjusting to the annual climatological precipitation of 995 mm in 2008 for Austria and 630 mm in 2000 for Switzerland. Longwave radiation was calculated using harmonized temperatures and humidities above (Brutsaert, 1975). Missing values were estimated via linear interpolation. Because soil temperature data were unavailable for local sites and for WFDEI, soil layer temperatures were calculated using the SEIB generator by regressing soil layer 1 on atmospheric temperature, soil layer 2 on layer 1, and layer 3 on layer 2. In Austria, humidity data were available from 2005. The WFDEI data were therefore used to estimate missing data via linear interpolation. In Canada, no observational data were available, except for temperature and precipitation. Precipitation in Canada was scaled with WFDEI data after adjusting to the total climatological precipitation for 1979–1984, shortwave radiation was taken from the WFDEI, and humidity data were harmonized in the same way as the humidity data in Austria.

2.3.1.3 Simulation scheme

To reach equilibrium conditions of the biomes, plant, and soil carbon pools, a 1000-year spin-up simulation was performed by looping the climate data and atmospheric CO_2 concentrations between 1979–2000. Building on the final conditions of the spin-up simulations, continuous simulations corresponding to 1979–2001 in Canada, 1979–2008 in Austria, 1979–2000 in Switzerland, and 1979–1995 in Panama were carried out, and the NSC dynamics were compared with field data.

https://doi.org/10.5194/egusphere-2022-835
Preprint. Discussion started: 5 October 2022

2.3.2 Validation at a global scale

In the global-scale simulation, the NSC seasonality in the SEIB-DGVM was validated using CRU/NCEP/MIROC integrated data (0.5 × 0.5 degrees, 1850-2100, Tei et al., 2017, Watanabe et al., 2011) as climatic input. SEIB-DGVM-NSC ver 1.0 is expected to simulate on future scenarios, thus the different climate data that cover longer period than that of section 2.3.1.2. are used for validation at a global scale. The SEIB-DGVM categorizes plant species into 16 PFTs for global-scale simulations.

For the validation, we used all available NSC data from the given climate zone. The outputs of the SEIB-DGVM include two boreal biome types (evergreen and deciduous forests), three temperate biome types (conifer, broad-leaved evergreen, and deciduous forests), and two tropical biome types (evergreen and deciduous forests), whereas the observations included two boreal biome types (conifer and deciduous forests), three temperate biome types (conifer, evergreen, and deciduous forests), and two tropical biome types (evergreen and deciduous forests). The model outputs and observation data were compared for each climate zone. Global climate data were available from 1850 to 2005. The first 30 years (1850–1880) were therefore looped for a 1000-year spin-up simulation. After the spin-up, simulations were run for the period 1850–2005. The NSC dynamics from the period 1975–2005 were used for model validation.

2.4 Parameterization of NSC functions

Hoch et al. (2003) have reported that the NSC_{leaf} of temperate trees varies between 7%–20% of the total leaf DM. They determined the seasonal mean of the NSC_{trunk} in sapwood of temperate deciduous trees and temperate evergreen trees to be 4.7% ± 0.1% of DM and 1.8% ± 0.1% of DM, respectively. There were no significant seasonal differences. The mean NSC_{root} was less than 1.5% of the root DM throughout the whole season (Gruber et al., 2012), and the total NSC of temperate trees was around 4%–5% of the DM during the growing season (Gruber et al., 2011). For tropical trees, the NSC_{trunk} and NSC_{root} were 8%–10% of their biomass, whereas the NSC_{leaf} fluctuated within 5%–9% of leaf biomass (Würth et al., 2005). Landhäusser and Lieffers (2003) have reported that the NSC_{root} of boreal trees, which is used to support leaf flush and root growth, is 3%–4% of their root mass. The stemwood NSC_{trunk} concentration is ~18 mg g^{-1} of the DM (Carbone et al., 2013). Because of limited observational data, the parameters of the NSC processes were derived mostly from the values observed at each site used for point-scale validation, and the maximums of simulated NSCs were corrected so that they were in the range of measured NSCs.

First, the parameter *b* in Eq. (10) was determined from the percentage of NSC and the biomass in January. The parameter *a* was then adjusted so that the fluctuations of the NSCs did not exceed

https://doi.org/10.5194/egusphere-2022-835
Preprint. Discussion started: 5 October 2022

the measured mean seasonal NSCs. The parameter a in Eq. (10) controls the minimum amount of photosynthetically fixed carbon mobilized for the NSC pools. In temperate zones, the value of a differs before and after July, and the NSC peaks around mid-summer. In contrast, in tropical zones, the amount of NSC in leaves and trunks decreases throughout the spring–summer.

Because the NSCs depend on the environmental conditions at the field sites, which could not be incorporated into the global simulation, different parameters were used when validating point-scale and global-scale results. Tables 3 and 4 show the parameters used for validation. Parameter values unrelated to the NSC module remain at the default values of the SEIB-DGVM (Sato et al., 2007).

Table 3. Parameters of NSC pool size function for point-scale simulation

Organ	Canada	Austria	Switzerland	Panama
Leaf	a: 0.4 × 10^{-3}, b: 0.09	a: 0.065 × 10^{-3}, b: 0.04 (Jul–Oct) a: 0.135 × 10^{-3}, b: 0.04 (others)	a: 0.1 × 10^{-3}, b: 0.13 (Jul–Oct) a: 0.8 × 10^{-3}, b: 0.13 (others)	a: 0.06, b: −0.15 × 10^{-3} (Jun–Nov) a: 0.06, b: 0.15 × 10^{-3} (others)
Trunk	a: 0.03 × 10^{-3}, b: 0.06	a: 0.05 × 10^{-3}, b: 0.02	a: 0.01 × 10^{-3}, b: 0.02	a: 0.1, b: −0.35 × 10^{-3} (Jun–Nov) a: 0.1, b: 0 (others)
Root	a: 0.06 × 10^{-3}, b: 0.14	a: 0.01 × 10^{-3}, b: 0.02	a: 0.003 × 10^{-3}, b: 0.06	a: 0.04, b: 0.005

Table 4. Parameters of NSC pool size functions for global-scale simulation

Organ	Boreal	Temperate	Tropical
Leaf	a: 0.4 × 10^{-3}, b: 0.09	a: 0.1 × 10^{-3}, b: 0.13 (Jul–Oct) a: 0.7 × 10^{-3}, b: 0.13 (others)	a: 0.06, b: −0.15 × 10^{-3} (May–Jul) a: 0.06, b: 0.15 × 10^{-3} (others)
Trunk	a: 0.03 × 10^{-3}, b: 0.06	a: 0.01 × 10^{-3}, b: 0.04	a: 0.1, b: −0.35 × 10^{-3}(May–Jul) a: 0.1, b: 0 (others)
Root	a: 0.06 × 10^{-3}, b: 0.14	a: 0.003 × 10^{-3}, b: 0.06	a: 0.06 × 10^{-3}, b: 0.0145

https://doi.org/10.5194/egusphere-2022-835
Preprint. Discussion started: 5 October 2022

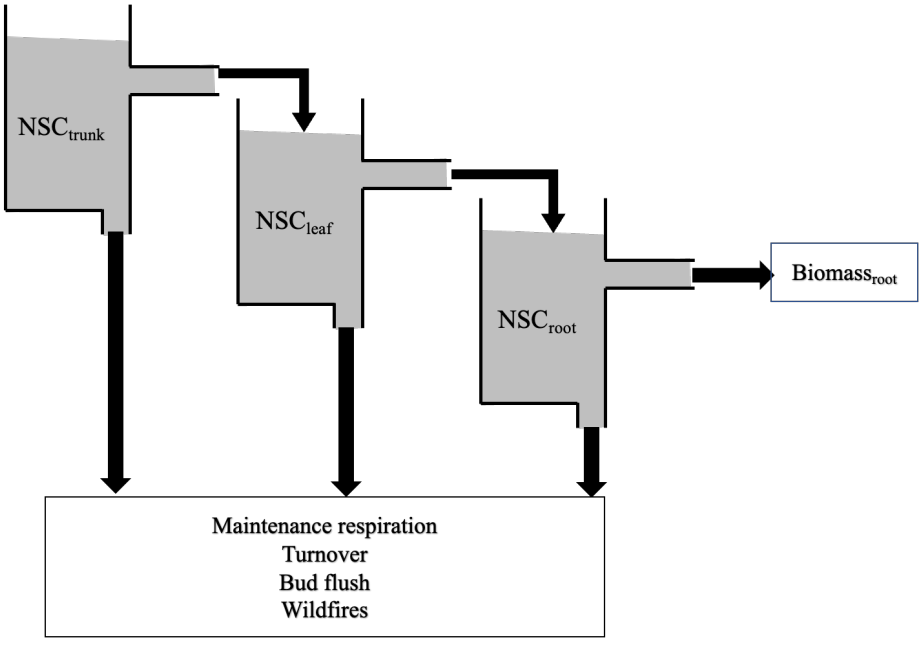

Figure 1. Schematic model structure of NSC pool.

https://doi.org/10.5194/egusphere-2022-835
Preprint. Discussion started: 5 October 2022

3 Results

3.1 Seasonality of NSC at the point scale

3.1.1 Canada

The fact that the dominant PFT in the simulations was boreal deciduous trees was consistent with observations at the site in Canada. The model simulated an increase in the NSC of leaves from 80 mg g^{-1} to 203 mg g^{-1}, whereas the observed NSC values were 89 mg g^{-1} in May and 185 mg g^{-1} in August (Fig. 2a). The modeled NSCs in leaves therefore captured the increasing trend during the growing season, but the simulations overestimated the maximum NSC a little. The observed NSCs in trunks fluctuated from 90 mg g^{-1} to 192 mg g^{-1} during a year with no specific seasonal trend (Fig. 2e). The model outputs in trunks were in the range 56–76 mg g^{-1}. Although the observed fluctuations exceeded the modeled outputs, the modeled outputs were within one standard deviation of the observations. The range of the observed NSCs in roots was 97–138 mg g^{-1}, whereas the range of the modeled NSCs was 117–132 mg g^{-1} (Fig. 2i). However, the observations peaked in August 2001 and in October 2002. The modeled NSCs of roots differed from the observed NSCs because the former peaked during August in both years. Overall, the simulated NSCs agreed well with the observed data (Fig. 3; RMSE = 69.92 mg g^{-1}, $r = 0.21$).

3.1.2 Austria

The fact that the dominant PFT in the simulations was temperate conifer forests was consistent with observations at the site in Austria. The modeled NSCs in leaves accumulated until July with a maximum of 142 mg g^{-1}. This pattern was similar to the observed seasonality of the NSCs, which peaked at 150 mg g^{-1} (Fig. 2b). The modeled NSCs in trunks were stable in the range 19–26 mg g^{-1}, and the observations were within the range 18–38 mg g^{-1}, with no specific seasonality (Fig. 2f). The modeled values were interspersed between the observations. The modeled NSCs in roots varied in a curvilinear manner from 18 to 26 mg g^{-1}, a range that was similar to the range of the observed NSCs, 13–32 mg g^{-1} (Fig. 2j). The seasonality and magnitudes of the modeled NSCs were consistent with observations (Fig. 3; RMSE = 9.52 mg g^{-1}, $r = 0.95$).

3.1.3 Switzerland

The dominant PFT in the simulations corresponded to the temperate conifers observed at the field site. The NSCs in the tree leaves accumulated during early spring and reached up to 222 mg g^{-1}

https://doi.org/10.5194/egusphere-2022-835
Preprint. Discussion started: 5 October 2022

(Fig. 2c). The decrease of the NSCs after July to a minimum of 135 mg g^{-1} was similar to the decline of the observed NSCs to a minimum of 124 mg g^{-1}. The modeled NSCs in trunks fell in the range 13–16 mg g^{-1}, which was overlapped with the range of the observed NSCs in trunks, 15–33 mg g^{-1} (Fig. 2g), and the modeled NSCs all fell within one standard deviation of the observations. The modeled NSCs in roots increased gradually from 45 to 62 mg g^{-1}, which is similar to the observed range of observations, 48–64 mg g^{-1} (Fig. 2k). The simulations captured the amounts and seasonal patterns of the NSCs in the different organs and produced results that compared well with observations (Fig. 3; RMSE = 25.83 mg g^{-1}, $r = 0.91$).

3.1.4 Panama

While a wide range of woody species was found at the Panama site, in the simulation the tropical evergreen PFT became dominant. The simulations showed that the NSCs in leaves were stored during winter and were then gradually consumed from July to October, when they reached a minimum of 52 mg g^{-1} (Fig. 2d). The observed NSCs in leaves likewise decreased from 69 to 48 mg g^{-1} between August and October. The model therefore followed the observed seasonality of the leaf NSCs. The modeled NSCs in trunks fell in the range 35–73 mg g^{-1} (Fig. 2h). The slight decrease of the modeled NSCs in trunks during the summer was not apparent in the observations. However, the simulated values fell within the range of the observed NSCs, 27–97 mg g^{-1}. The simulated NSCs in roots fell in the range 23–55 mg g^{-1}; the observed NSCs ranged from 43 to 70 mg g^{-1} (Fig. 2l). Despite the weak correlation between simulated and observed NSCs, the model results were within the acceptable margin of error (Fig. 3; RMSE = 20.75 mg g^{-1}, $r = 0.08$).

3.2 Seasonality at a global scale

For validation at a global scale, the mean annual NSCs from the model were compared with the observed mean annual NSCs in boreal, temperate, and tropical regions (Table 5). The model simulated the amounts of NSCs in forest tree trunks in all climate regions with high accuracy. The modeled NSCs in the trunks of trees in boreal forests averaged 47.48 ± 18.35 mg g^{-1}, which compared favorably with the observed average of 76.67 ± 23.68 mg g^{-1}. In temperate forests, the modeled NSCs of trunks averaged 44.78 ± 6.82 mg g^{-1}, which was close to the observed average of 51.59 ± 22.63 mg g^{-1}. The modeled NSCs of trunks in tropical forests averaged 66.68 ± 18.79 mg g^{-1}, which was close to the average of the observations, 106.23 ± 32.52 mg g^{-1}. Although the modeled NSCs in leaves of temperate and tropical forests were close to observed values, the modeled NSCs in leaves of boreal forests underestimated the observed values. Moreover, the modeled NSCs in roots of tropical forests were smaller than the observed NSCs. Overall, the simulated NSCs of all

https://doi.org/10.5194/egusphere-2022-835
Preprint. Discussion started: 5 October 2022

organs of forest trees in all climate regions agreed reasonably well with observations (Fig. 4; RMSE = 66.75 mg g^{-1}, r = 0.17). The model could simulate the NSCs with high accuracy, with the exception of the NSCs of tree leaves in boreal forests and of tree roots in tropical forests (Fig. 4; RMSE = 34.15 mg g^{-1}, r = 0.71).

Table 5. Comparison of modelled and observed annual mean NSC concentrations (mg g^{-1}) on a global scale. The observed results are represented as the mean ± 1 standard deviation

	Boreal		Temperate		Tropical	
	Observation	Model	Observation	Model	Observation	Model
Leaf	202.80 ± 19.97	94.91 ± 42.91	127.10 ± 25.6	170.90 ± 46.54	86.42 ± 20.21	46.92 ± 16.20
Trunk	76.67 ± 23.68	47.48 ± 18.35	51.59 ± 22.63	44.78 ± 6.82	106.23 ± 32.52	66.68 ± 18.79
Root	118.49 ± 13.24	105.80 ± 40.82	67.65 ± 18.79	23.58 ± 10.57	170.40 ± 36.49	44.55 ± 15.15

3.3 Woody biomass and total NSCs on a global scale

The average of the total GPP simulated from the new model during 1976–2005 was 123 PgC $year^{-1}$. The model estimated the mean total woody biomass to be 282 PgC $year^{-1}$ in boreal zones, 100 PgC $year^{-1}$ in temperate zones, and 337 PgC $year^{-1}$ in tropical zones globally during 1976–2005. In boreal zones such as North America and Russia, the mean concentration of total NSCs was 4.98% ± 1.87% of total woody biomass (Fig. 5). In temperate zones such as Asia, the mean concentration of total NSCs was 4.67% ± 0.54% of total woody biomass. Total NSCs of tropical forests in South America and Africa were 6.19% ± 1.66% of their total woody biomass. Mean values of the simulated total NSCs relative to total woody biomass were close to previous estimates for temperate and tropical forests (Table 6). The total NSCs of temperate, broad-leaved, evergreen forests were 4.63% ± 0.50% of the corresponding woody biomass reported by Smith et al. (2018). The total NSCs of temperate conifer forests were 4.72% ± 0.58% of total woody biomass, which was close to the figure of 4% reported by Körner (2003). According to Würth et al. (2005), the percentages of woody biomass contributed by NSCs are 4%–8% in tropical forests, 4.66% ± 1.28% in tropical deciduous forests, and 7.11% ± 1.08% in tropical evergreen forests. These observed percentages are close to our simulated values.

Table 6. Comparison of modeled mean NSC concentrations to observed total NSC concentrations (%) for different types of biomes. The simulated results are expressed as the mean ± 1 standard deviation

https://doi.org/10.5194/egusphere-2022-835
Preprint. Discussion started: 5 October 2022

	Total NSC	Leaf	Trunk	Root	Observation
Boreal deciduous	3.41 ± 1.58	0.05 ± 0.09	3.06 ± 1.23	0.30 ± 0.62	
Boreal evergreen	6.06 ± 1.16	0.75 ± 0.38	4.73 ± 1.29	0.58 ± 0.37	
Temperate deciduous	2.30 ± 0.33	0.02 ± 0.01	2.25 ± 0.31	0.03 ± 0.01	1.0–12.5 (Gough et al., 2009)
Temperate broad-leaved evergreen	4.63 ± 0.50	0.49 ± 0.20	4.10 ± 0.56	0.04 ± 0.03	2.6–4.4 (Smith et al., 2018)
Temperate conifer	4.72 ± 0.58	0.89 ± 0.38	3.77 ± 0.73	0.08 ± 0.04	4.0 (Körner, 2003)
Tropical deciduous	4.66 ± 1.28	0.04 ± 0.03	4.60 ± 1.27	0.03 ± 0.02	4.0–8.0 (Würth et al., 2005)
Tropical evergreen	7.11 ± 1.08	0.08 ± 0.03	7.00 ± 1.08	0.02 ± 0.01	4.0–8.0 (Würth et al., 2005)

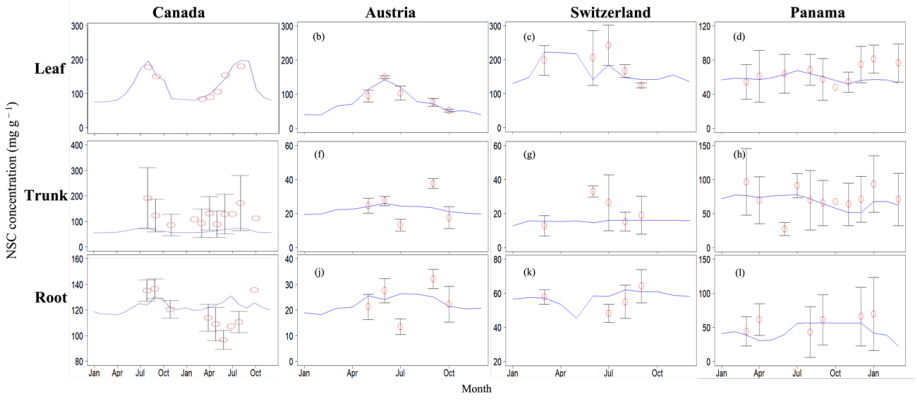

Figure 2. Validation of the modeled NSC with observed NSC data (mg g^{-1}) at sites in Canada, Austria, Switzerland, and Panama. Red circles indicate the observed data, and blue lines indicate the modeled NSC. The observed results are represented as mean ± 1 standard deviation.

https://doi.org/10.5194/egusphere-2022-835
Preprint. Discussion started: 5 October 2022

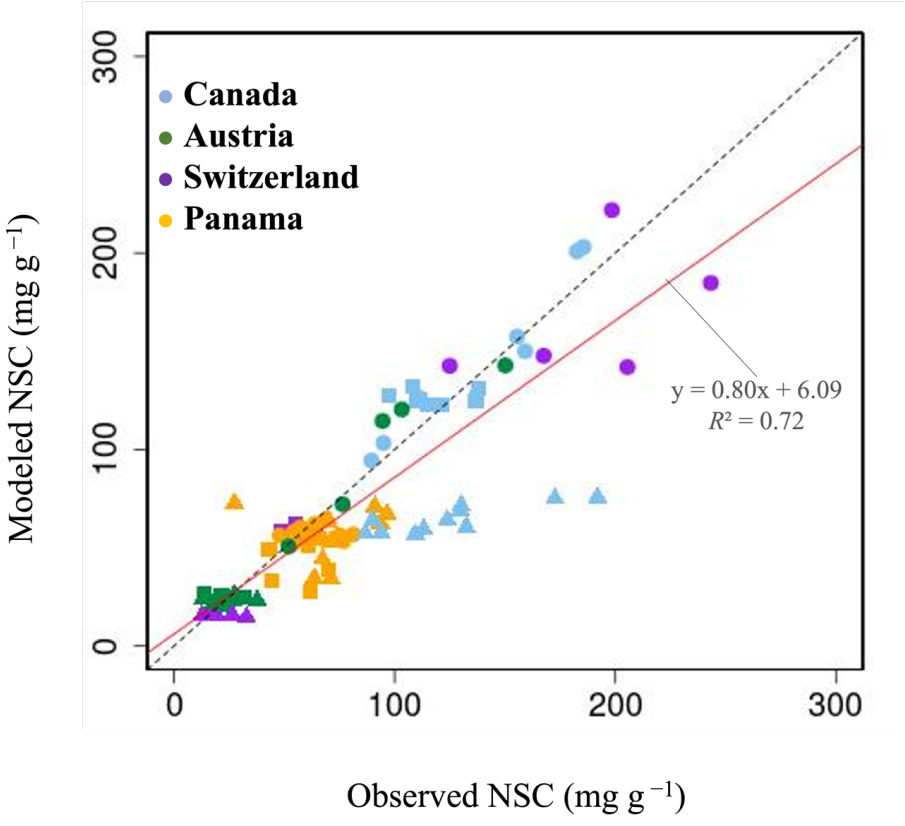

Figure 3. Plot of modeled NSC (mg g^{-1}) with observed NSC (mg g^{-1}) at a point scale. ●, leaves; ▲, trunks; ■, roots. For all data, *r* is 0.72, and RMSE is 29.65 mg g^{-1}.

https://doi.org/10.5194/egusphere-2022-835
Preprint. Discussion started: 5 October 2022

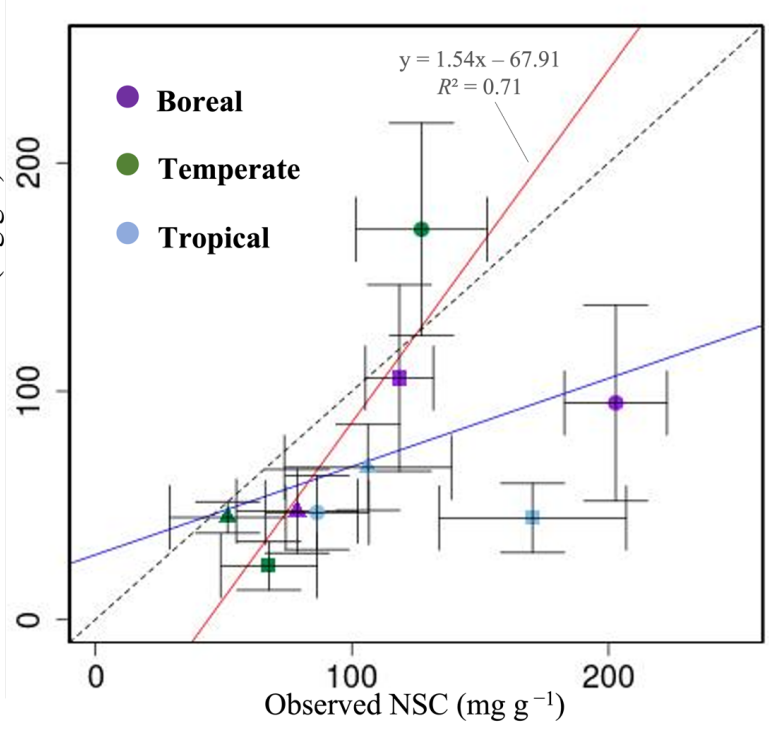

536

537 **Figure 4.** Plot of modeled NSC (mg g^{-1}) with observed NSC (mg g^{-1}) at a global scale. ●, leaves;
538 ▲, trunks; ■, roots.

539

https://doi.org/10.5194/egusphere-2022-835
Preprint. Discussion started: 5 October 2022

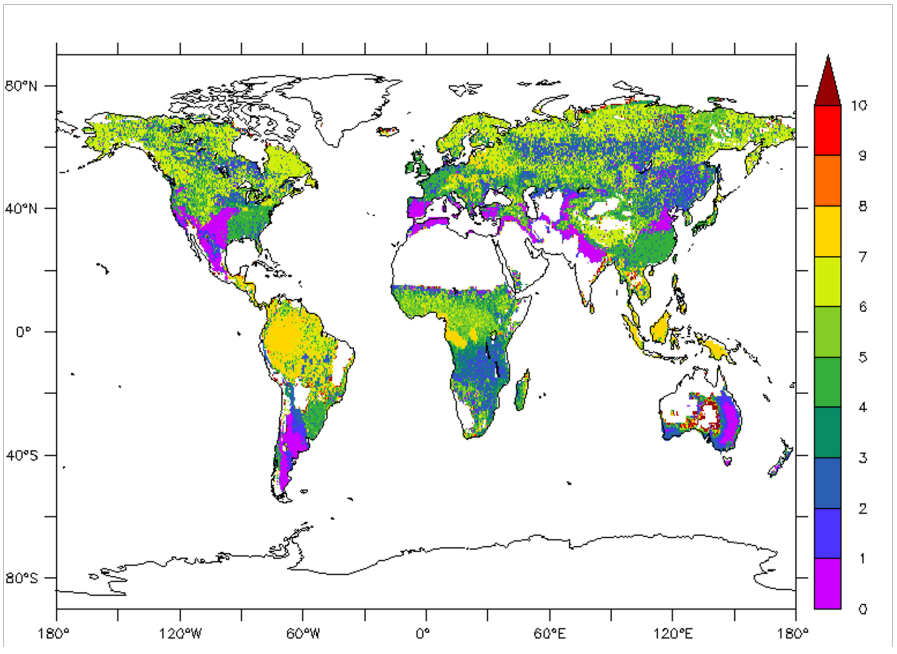

Figure 5. Mean total NSC concentration relative to total woody biomass during 1976–2005 (%).

https://doi.org/10.5194/egusphere-2022-835
Preprint. Discussion started: 5 October 2022

4 Discussion

On a point scale, the modeled NSCs for boreal forests in Canada were close to the observed NSCs. The seasonality of the modeled NSCs in leaves was consistent with observations. However, the seasonality of NSC in roots differed from the observations because there were insufficient observations in boreal regions that enabled assessment of the seasonality of NSCs in all organs. The seasonality of NSCs in roots is therefore still unclear. In temperate zones, the model simulated the observed NSCs very accurately. The simulated NSCs of temperate forests were close to observed values in Austria and Switzerland. The simulations showed that the NSCs in leaves were consumed in winter for bud flush, and the leaves accumulated NSCs during the growing season. This pattern corresponded to the seasonality reported in Asaadi et al. (2018) and Furze et al. (2019). In the tropical zones, the model also captured a seasonality of NSCs that was similar to observations. The NSC concentration in the canopy of tropical forests decreased from June to August to satisfy increased maintenance demands (Signori-Müller et al., 2022; Würth et al., 2005). The simulated NSCs in leaves followed a similar pattern from June to August, and the simulated NSCs in leaves, trunks, and roots were close to observed values.

On a global scale, the simulated NSC values of all climate regions agreed with the observed data, except for the leaves of boreal forests and roots of tropical forests. The new function, which was validated at the point scale, could therefore perform well on a global scale. The NSCs in trunks, which contain the greatest amounts of carbon in trees, were simulated accurately in all climate regions. The new function could therefore calculate the total NSC storage in trees with great accuracy.

The model with the new function calculated the global GPP to be 123 PgC year^{-1}, which is close to the previous estimates of 106.2 ± 2.9 PgC year^{-1} by Zheng et al. (2020) and 130 ± 1.6 PgC year^{-1} by Madani et al. (2020). Moreover, the simulated mean total woody biomass for boreal forests was 282 PgC year^{-1}, which is within the range of 249–295 PgC year^{-1} reported by Pan et al. (2011). The simulated woody biomass of 100 PgC year^{-1} for temperate forests was within the observed range of 59–139 PgC year^{-1} (Hui et al., 2020) and a little lower than the range of 113–125 PgC year^{-1} for other temperate forests (Pan et al., 2011). The calculated total woody biomass of 337 PgC year^{-1} for tropical forests was within the range of 212–340 PgC year^{-1} reported by Hui et al. (2020) and was not very different from the estimates of 378–564 PgC year^{-1} by Pan et al. (2011), and 200–300 PgC year^{-1} by Mitchard (2018). Furthermore, the total NSCs relative to total biomass output from the new function for temperate and tropical biome types agreed with previous research. The total NSC of boreal biome types could not be compared with observations due to lack of data.

The new model has a high potential to simulate various biotic effects on terrestrial ecosystems

https://doi.org/10.5194/egusphere-2022-835
Preprint. Discussion started: 5 October 2022

more accurately by calculating the NSC dynamics within each plant organ. The NSCs stored in the trunk and roots compensate for the deficit of CO_2 uptake in trees under stress, and the NSC stored in roots is potentially indispensable for tree recovery after disturbances (Herrera-Ramírez et al., 2020). Furthermore, the NSC changes in the trunk and roots are better indicators of carbon source–sink relationships under elevated CO_2 conditions than the NSC changes in leaves because the NSC concentrations in leaves increase under elevated CO_2 conditions irrespective of growth conditions. The NSC changes in the trunk and roots are therefore more tied to the carbon balance of plant bodies (Körner, 2003). Simulation of the dynamics of NSC in the three compartments in this research contributes to understanding plant growth and the response of carbon dynamics in each organ to increasing atmospheric CO_2.

Carbon starvation may also be the main cause of plant death during drought when photosynthesis decreases and water stress increases (McDowell et al., 2008). If reduced photosynthetic rates cannot supply enough carbon for NSC accumulation during drought, there will be greater canopy dieback in the next season. Plants therefore prioritize NSC storage, even when no excess carbon is available (Hartmann et al., 2020). At times, plants are unable to allocate carbon for this NSC defense mechanism, and their reduced ability to recover from biotic attacks such as defoliation caused by insect pests leads to decreased growth rates, less restoration of NSC, and lower survival rates. These processes may culminate in broad-scale tree mortalities (McDowell, 2011; Chen et al., 2017).

The new model introduced NSC compartments in leaves, trunk, and roots that were validated at the point and global scales. Use of the model developed here enabled simulation of the environmental effects on forests resulting from the changing amount of NSC in each organ. The simulations depicted the NSC changes in the trunk especially well. The model could thus be used as an indicator of the carbon cycle in terrestrial ecosystems to understand the effect of climate change. Simulation of photosynthetic carbon allocated into NSC storage in leaves, trunks, and roots enables a more dynamic simulation of the carbon cycle between terrestrial ecosystems and the atmosphere.

However, there were still some limitations to this research. We considered two potential limitations that could lead to some discrepancies between the modeled and measured NSC values. First, the relatively coarse spatial resolution of 0.5°×0.5° gridded climate data at the global scale could not depict the details of local climates derived from observations. These differences were especially important in the case of precipitation and soil properties, which play a key role in NSC dynamics. Lowering of the water level in soils causes damage to the hydraulic conductivity of the phloem tube, which leads to a decline of phloem conductance at the stem level (Dannoura et al., 2018; Sevanto, 2014). This cessation of phloem transport could change the allocation of photosynthetic products to plant growth and affect the ability of the trees to accumulate NSCs

https://doi.org/10.5194/egusphere-2022-835
Preprint. Discussion started: 5 October 2022

(Dannoura et al., 2018).

Second, the scarcity of ground-measured NSC seasonality prevented us from having more average information on NSC concentrations, especially in the tropical and boreal regions, where there were fewer available data. The NSC seasonality differs between biome types, but because it is difficult to measure NSC dynamics, there is a lack of long-term data for each biome type. Hence, parameters were tuned to simulate the same seasonality for all the biome types in a given climate zone in our study. The fact that the NSC allocation was further influenced by environmental conditions caused the allocation patterns to change within the same biome type. The NSC allocation to roots was favored over aboveground allocations when soil resources were lacking, and tree size was considered an important determinant of carbon allocation as well as aridity (Hartmann et al., 2020). Because we pooled data for each organ from different measurement sites for global-scale validation, environmental effects on the data could not be measured. In addition to the above factors, the number of samples and duration of observations differed between the various studies. These differences led to no explicit NSC seasonality. These potential sources of error in the field measurements jeopardized the model performances.

5 Conclusions

In this study, a new NSC model was incorporated into the SEIB-DGVM to understand the effect of NSC allocation on global forest dynamics through competition and establishment among individual trees. The new module calculated the NSC dynamics of three organs—leaves, trunk, and roots—and the general NSC seasonality based on ground measurements was determined for biome types in three climate zones: boreal, temperate, and tropical. The NSC seasonality was validated at four sites: Canada (boreal), Austria and Switzerland (temperate), and Panama (tropical). The mean values of simulated NSC concentration agreed reasonably well with observed data on a global scale.

The model enabled us to simulate the biotic effects resulting from insufficient NSC caused by factors such as carbon starvation and insect pests that are otherwise difficult to measure in terrestrial ecosystems globally. The difference of the NSC dynamics in the organs under elevated CO_2 conditions highlighted the importance of modeling the organs separately when studying environmental stresses. As more observation data about NSC dynamics become available, the model can be further improved and can contribute to the simulations of the passive biome shifts that may occur globally.

Code and data availability

The model code used in this study is archived at https://doi.org/10.5281/zenodo.7021459.

https://doi.org/10.5194/egusphere-2022-835
Preprint. Discussion started: 5 October 2022

Author contributions. T.K. conceived and supervised this study and acquired the funding. H.N. developed the model code and carried out the analysis and produced the figures. H.N. prepared the original draft, and T.K., and L.V. reviewed it. L.W. prepared the modeling environment. All authors have read and agreed to the published version of the manuscript.

Competing interests. The authors declare that they have no conflicts of interest.

Acknowledgments. This study was funded by the Nippon Life Insurance Company. This work was supported by JSPS KAKENHI Grant Number JP 22J20286.
We thank all the contributors. Dr. Epron and Dr. Dannoura in Kyoto University provided assistance. Dr. Hajima and Dr. Mori converted MIROC and CRU/NCEP climate data for CRU/NCEP/MIROC integrated data. We acknowledge the data provided by the European Climate Assessment & Dataset project.

References

Adams, H. D., Germino, M. J., Breshears, D. D., Barron-Gafford, G. A., Guardiola-Claramonte, M., Zou, C. B. and Huxman, T. E.: Nonstructural leaf carbohydrate dynamics of *Pinus edulis* during drought-induced tree mortality reveal role for carbon metabolism in mortality mechanism, New Phytol., 197(4), 1142–1151, doi:10.1111/nph.12102, 2013.

Adams, H. D., Zeppel, M. J. B., Anderegg, W. R. L., Hartmann, H., Landhäusser, S. M., Tissue, D. T., Huxman, T. E., Hudson, P. J., Franz, T. E., Allen, C. D., Anderegg, L. D. L., Barron-Gafford, G. A., Beerling, D. J., Breshears, D. D., Brodribb, T. J., Bugmann, H., Cobb, R. C., Collins, A. D., Dickman, L. T., Duan, H., Ewers, B. E., Galiano, L., Galvez, D. A., Garcia-Forner, N., Gaylord, M. L., Germino, M. J., Gessler, A., Hacke, U. G., Hakamada, R., Hector, A., Jenkins, M. W., Kane, J. M., Kolb, T. E., Law, D. J., Lewis, J. D., Limousin, J. M., Love, D. M., Macalady, A. K., Martínez-Vilalta, J., Mencuccini, M., Mitchell, P. J., Muss, J. D., O'Brien, M. J., O'Grady, A. P., Pangle, R. E., Pinkard, E. A., Piper, F. I., Plaut, J. A., Pockman, W. T., Quirk, J., Reinhardt, K., Ripullone, F., Ryan, M. G., Sala, A., Sevanto, S., Sperry, J. S., Vargas, R., Vennetier, M., Way, D. A., Xu, C., Yepez, E. A. and McDowell, N. G.: A multi-species synthesis of physiological mechanisms in drought-induced tree mortality, Nat. Ecol. Evol., 1(9), 1285–1291, doi:10.1038/s41559-017-0248-x, 2017.

Asaadi, A., Arora, V. K., Melton, J. R. and Bartlett, P.: An improved parameterization of leaf area

https://doi.org/10.5194/egusphere-2022-835
Preprint. Discussion started: 5 October 2022

688 index (LAI) seasonality in the Canadian Land Surface Scheme (CLASS) and Canadian
689 Terrestrial Ecosystem Model (CTEM) modelling framework, Biogeosciences, 15(22), 6885–
690 6907, doi:10.5194/bg-15-6885-2018, 2018.
691
692 Braakhekke, M. C., Doelman, J. C., Baas, P., Müller, C., Schaphoff, S., Stehfest, E. and Van
693 Vuuren, D. P.: Modeling forest plantations for carbon uptake with the LPJmL dynamic global
694 vegetation model, Earth Syst. Dyn., 10(4), 617–630, doi:10.5194/esd-10-617-2019, 2019.
695
696 Brutsaert, W.: On a derivable formula for long - wave radiation from clear skies, Water Resour.
697 Res., 11(5), 742-744, doi:10.1029/WR011i005p00742, 1975.
698
699 Carbone, M. S., Czimczik, C. I., Keenan, T. F., Murakami, P. F., Pederson, N., Schaberg, P. G.,
700 Xu, X. and Richardson, A. D.: Age, allocation and availability of nonstructural carbon in
701 mature red maple trees, New Phytol., 200(4), 1145–1155, doi:10.1111/nph.12448, 2013.
702
703 Chen, Z., Wang, L., Dai, Y., Wan, X. and Liu, S.: Phenology-dependent variation in the non-
704 structural carbohydrates of broadleaf evergreen species plays an important role in determining
705 tolerance to defoliation (or herbivory), Sci. Rep., 7(1), 1–11, doi:10.1038/s41598-017-09757-
706 2, 2017.
707
708 Chuste, P. A., Maillard, P., Bréda, N., Levillain, J., Thirion, E., Wortemann, R. and Massonnet,
709 C.: Sacrificing growth and maintaining a dynamic carbohydrate storage are key processes for
710 promoting beech survival under prolonged drought conditions, Trees - Struct. Funct., 34(2),
711 381–394, doi:10.1007/s00468-019-01923-5, 2020.
712
713 Dannoura, M., Epron, D., Desalme, D., Massonnet, C., Tsuji, S., Plain, C., Priault, P. and Gérant,
714 D.: The impact of prolonged drought on phloem anatomy and phloem transport in young
715 beech trees, Tree Physiol., 39(2), 201–210, doi:10.1093/treephys/tpy070, 2018.
716
717 Dietze, M. C., Sala, A., Carbone, M. S., Czimczik, C. I., Mantooth, J. A., Richardson, A. D. and
718 Vargas, R.: Nonstructural carbon in woody plants, Annu. Rev. Plant Biol., 65(June 2014),
719 667–687, doi:10.1146/annurev-arplant-050213-040054, 2014.
720
721 Furze, M. E., Huggett, B. A., Aubrecht, D. M., Stolz, C. D., Carbone, M. S. and Richardson, A.
722 D.: Whole-tree nonstructural carbohydrate storage and seasonal dynamics in five temperate
723 species, New Phytol., 221(3), 1466–1477, doi:10.1111/nph.15462, 2019.

https://doi.org/10.5194/egusphere-2022-835
Preprint. Discussion started: 5 October 2022

Gough, C. M., Flower, C. E., Vogel, C. S. and Curtis, P. S.: Phenological and temperature controls on the temporal non-structural carbohydrate dynamics of *Populus grandidentata* and *Quercus rubra*, Forests, 1(1), 65–81, doi:10.3390/f1010065, 2010.

Gough, C. M., Flower, C. E., Vogel, C. S., Dragoni, D. and Curtis, P. S.: Whole-ecosystem labile carbon production in a north temperate deciduous forest, Agric. For. Meteorol., 149(9), 1531–1540, doi:10.1016/j.agrformet.2009.04.006, 2009.

Gruber, A., Pirkebner, D., Oberhuber, W. and Wieser, G.: Spatial and seasonal variations in mobile carbohydrates in Pinus cembra in the timberline ecotone of the Central Austrian Alps, Eur. J. For. Res., 130(2), 173–179, doi:10.1007/s10342-010-0419-7, 2011.

Gruber, A., Pirkebner, D., Florian, C. and Oberhuber, W.: No evidence for depletion of carbohydrate pools in Scots pine (Pinus sylvestris L.) under drought stress, Plant Biol., 14(1), 142–148, doi:10.1111/j.1438-8677.2011.00467.x, 2012.

Harris, I., P. D. Jones, T. J. Osborn, and D. H. Lister: Updated high-resolution grids of monthly climatic observations - the CRU TS3.10 Dataset, Int. J. Climatol., 34(3), 623-642, doi:10.1002/joc.3711, 2014.

Hartmann, H., Adams, H. D., Hammond, W. M., Hoch, G., Landhäusser, S. M., Wiley, E. and Zaehle, S.: Identifying differences in carbohydrate dynamics of seedlings and mature trees to improve carbon allocation in models for trees and forests, Environ. Exp. Bot., 152(September 2017), 7–18, doi:10.1016/j.envexpbot.2018.03.011, 2018.

Hartmann, H., Bahn, M., Carbone, M. and Richardson, A. D.: Plant carbon allocation in a changing world – challenges and progress: introduction to a Virtual Issue on carbon allocation: Introduction to a virtual issue on carbon allocation, New Phytol., 227(4), 981–988, doi:10.1111/nph.16757, 2020.

He, W., Liu, H., Qi, Y., Liu, F. and Zhu, X.: Patterns in nonstructural carbohydrate contents at the tree organ level in response to drought duration, Glob. Chang. Biol., 26(6), 3627–3638, doi:10.1111/gcb.15078, 2020.

Herrera-Ramírez, D., Muhr, J., Hartmann, H., Römermann, C., Trumbore, S. and Sierra, C. A.:

https://doi.org/10.5194/egusphere-2022-835
Preprint. Discussion started: 5 October 2022

760 Probability distributions of nonstructural carbon ages and transit times provide insights into
761 carbon allocation dynamics of mature trees, New Phytol., 226(5), 1299‐1311,
762 doi:10.1111/nph.16461, 2020.
763
764 Hickler, T., Smith, B., Sykes, M. T., Davis, M. B., Sugita, S. and Walker, K.: Using a generalized
765 vegetation model to simulate vegetation dynamics in northeastern USA, Ecology, 85(2), 519–
766 530, doi:10.1890/02-0344, 2004.
767
768 Hoch, G., Richter, A. and Körner, C.: Non-structural carbon compounds in temperate forest trees,
769 Plant, Cell Environ., 26(7), 1067–1081, doi:10.1046/j.0016-8025.2003.01032.x, 2003.
770
771 Huang, J., Kautz, M., Trowbridge, A. M., Hammerbacher, A., Raffa, K. F., Adams, H. D.,
772 Goodsman, D. W., Xu, C., Meddens, A. J. H., Kandasamy, D., Gershenzon, J., Seidl, R. and
773 Hartmann, H.: Tree defence and bark beetles in a drying world: carbon partitioning,
774 functioning and modelling, New Phytol., 225(1), 26–36, doi:10.1111/nph.16173, 2020.
775
776 Hui, D., Deng, Q., Tian, H. and Luo, Y.: Handbook of Climate Change Mitigation and Adaptation.,
777 2020.
778
779 IPCC: 2014: Climate Change 2014: Synthesis Report. Contribution of Working Groups I, II and
780 III to the Fifth Assessment Report of the Intergovernmental Panel on Climate Change, edited
781 by: Core Writing Team, Pachauri, R. K., and Meyer, L. A., IPCC, Geneva, Switzerland, 2014.
782
783 Jones, S., Rowland, L., Cox, P., Hemming, D., Wiltshire, A., Williams, K., Parazoo, N., Liu, J.,
784 da Costa, A., Meir, P., Mencuccini, M. and Harper, A.: The Impact of a Simple Representation
785 of Non-Structural Carbohydrates on the Simulated Response of Tropical Forests to Drought,
786 Biogeosciences Discuss., 1–26, doi:10.5194/bg-2019-452, 2019.
787
788 Kalnay, E., Kanamitsu, M., Kistler, R., Collins, W., Deaven, D., Gandin, L., Iredell, M.,
789 Saha, S., White, G., Woollen, J., Zhu, Y., Chelliah, M., Ebisuzaki, W., Higgins, W.,
790 Janowiak, J., Mo, K. C., Ropelewski, C., Wang, J., Leetmaa, A., Reynolds, R.,
791 Jenne, R., & Joseph, D.: The NCEP/NCAR 40-Year Reanalysis Project, Bulletin of
792 the American Meteorological Society, 77(3), 437-472. 1996
793
794 Klein, T. and Hoch, G.: Tree carbon allocation dynamics determined using a carbon mass balance
795 approach, New Phytol., 205(1), 147–159, doi:10.1111/nph.12993, 2015.

https://doi.org/10.5194/egusphere-2022-835
Preprint. Discussion started: 5 October 2022

Klein Tank, A.M.G. and Coauthors, 2002. Daily dataset of 20th-century surface air temperature and precipitation series for the European Climate Assessment. Int. J. of Climatol., 22, 1441-1453.

Körner, C.: Carbon limitation in trees, J. Ecol., 91(1), 4–17, doi:10.1046/j.1365-2745.2003.00742.x, 2003.

Krinner, G., Viovy, N., de Noblet-Ducoudré, N., Ogée, J., Polcher, J., Friedlingstein, P., Ciais, P., Sitch, S. and Prentice, I. C.: A dynamic global vegetation model for studies of the coupled atmosphere-biosphere system, Global Biogeochem. Cycles, 19(1), 1–33, doi:10.1029/2003GB002199, 2005.

Landhäusser, S. M. and Lieffers, V. J.: Seasonal changes in carbohydrate reserves in mature northern Populus tremuloides clones, Trees - Struct. Funct., 17(6), 471–476, doi:10.1007/s00468-003-0263-1, 2003.

Madani, N., Parazoo, N. C., Kimball, J. S., Ballantyne, A. P., Reichle, R. H., Maneta, M., Saatchi, S., Palmer, P. I., Liu, Z. and Tagesson, T.: Recent Amplified Global Gross Primary Productivity Due to Temperature Increase Is Offset by Reduced Productivity Due to Water Constraints, AGU Adv., 1(4), doi:10.1029/2020av000180, 2020.

Martínez-Vilalta, J., Sala, A., Asensio, D., Galiano, L., Hoch, G., Palacio, S., Piper, F. I. and Lloret, F.: Dynamics of non-structural carbohydrates in terrestrial plants: A global synthesis, Ecol. Monogr., 86(4), 495–516, doi:10.1002/ecm.1231, 2016.

McDowell, N., Pockman, W. T., Allen, C. D., Breshears, D. D., Cobb, N., Kolb, T., Plaut, J., Sperry, J., West, A., Williams, D. G. and Yepez, E. A.: Mechanisms of plant survival and mortality during drought: Why do some plants survive while others succumb to drought?, New Phytol., 178(4), 719–739, doi:10.1111/j.1469-8137.2008.02436.x, 2008.

McDowell, N. G.: Mechanisms linking drought, hydraulics, carbon metabolism, and vegetation mortality, Plant Physiol., 155(3), 1051–1059, doi:10.1104/pp.110.170704, 2011.

McDowell, N. G., Allen, C. D., Anderson-Teixeira, K., Aukema, B. H., Bond-Lamberty, B., Chini, L., Clark, J. S., Dietze, M., Grossiord, C., Hanbury-Brown, A., Hurtt, G. C., Jackson, R. B.,

https://doi.org/10.5194/egusphere-2022-835
Preprint. Discussion started: 5 October 2022

Johnson, D. J., Kueppers, L., Lichstein, J. W., Ogle, K., Poulter, B., Pugh, T. A. M., Seidl, R., Turner, M. G., Uriarte, M., Walker, A. P. and Xu, C.: Pervasive shifts in forest dynamics in a changing world, Science (80-.)., 368(6494), doi:10.1126/science.aaz9463, 2020.

Mitchard, E. T. A.: The tropical forest carbon cycle and climate change, Nature, 559(7715), 527–534, doi:10.1038/s41586-018-0300-2, 2018.

Pan, Y., Birdsey, R. A., Fang, J., Houghton, R., Kauppi, P. E., Kurz, W. A., Phillips, O. L., Shvidenko, A., Lewis, S. L., Canadell, J. G., Ciais, P., Jackson, R. B., Pacala, S. W., McGuire, A. D., Piao, S., Rautiainen, A., Sitch, S., and Hayes, D.: A large and persistent carbon sink in the world's forests, Science (1979), 333, 988–993, doi:10.1126/science.1201609, 2011.

Rademacher, T., Fonti, P., LeMoine, J. M., Fonti, M. V., Basler, D., Chen, Y., Friend, A. D., Seyednasrollah, B., Eckes-Shephard, A. H. and Richardson, A. D.: Manipulating phloem transport affects wood formation but not local nonstructural carbon reserves in an evergreen conifer, Plant Cell Environ., 44(8), 2506–2521, doi:10.1111/pce.14117, 2021.

Richardson, A. D., Carbone, M. S., Keenan, T. F., Czimczik, C. I., Hollinger, D. Y., Murakami, P., Schaberg, P. G. and Xu, X.: Seasonal dynamics and age of stemwood nonstructural carbohydrates in temperate forest trees, New Phytol., 197(3), 850–861, doi:10.1111/nph.12042, 2013.

Sala, A., Woodruff, D. R. and Meinzer, F. C.: Carbon dynamics in trees: Feast or famine?, Tree Physiol., 32(6), 764–775, doi:10.1093/treephys/tpr143, 2012.

Sato, H. and Ise, T.: Effect of plant dynamic processes on African vegetation responses to climate change: Analysis using the spatially explicit individual-based dynamic global vegetation model (SEIB-DGVM), J. Geophys. Res. Biogeosciences, 117(3), 1–18, doi:10.1029/2012JG002056, 2012.

Sato, H., Itoh, A. and Kohyama, T.: SEIB-DGVM: A new Dynamic Global Vegetation Model using a spatially explicit individual-based approach, Ecol. Modell., 200(3–4), 279–307, doi:10.1016/j.ecolmodel.2006.09.006, 2007.

Sato, H., Kobayashi, H., Beer, C. and Fedorov, A.: Simulating interactions between topography,

https://doi.org/10.5194/egusphere-2022-835
Preprint. Discussion started: 5 October 2022

permafrost, and vegetation in Siberian larch forest, Environ. Res. Lett., 15(9), doi:10.1088/1748-9326/ab9be4, 2020.

Sato, H., Kobayashi, H., Iwahana, G., and Ohta, T.: Endurance of larch forest ecosystems in eastern Siberia under warming trends, Ecol. Evol., 6, 5690–5704, https://doi.org/10.1002/ece3.2285, 2016.

Seidl, R., Thom, D., Kautz, M., Martin-Benito, D., Peltoniemi, M., Vacchiano, G., Wild, J., Ascoli, D., Petr, M., Honkaniemi, J., Lexer, M. J., Trotsiuk, V., Mairota, P., Svoboda, M., Fabrika, M., Nagel, T. A. and Reyer, C. P. O.: Forest disturbances under climate change, Nat. Clim. Chang., 7(6), 395–402, doi:10.1038/nclimate3303, 2017.

Sevanto, S.: Phloem transport and drought, J. Exp. Bot., 65(7), 1751–1759, doi:10.1093/jxb/ert467, 2014.

Sevanto, S. and Dickman, L. T.: Where does the carbon go?-Plant carbon allocation under climate change, Tree Physiol., 35(6), 581–584, doi:10.1093/treephys/tpv059, 2015.

Signori-Müller, C., Oliveira, R. S., Valentim Tavares, J., Carvalho Diniz, F., Gilpin, M., de V. Barros, F., Marca Zevallos, M. J., Salas Yupayccana, C. A., Nina, A., Brum, M., Baker, T. R., Cosio, E. G., Malhi, Y., Monteagudo Mendoza, A., Phillips, O. L., Rowland, L., Salinas, N., Vasquez, R., Mencuccini, M. and Galbraith, D.: Variation of non-structural carbohydrates across the fast–slow continuum in Amazon Forest canopy trees, Funct. Ecol., 36(2), 341–355, doi:10.1111/1365-2435.13971, 2022.

Singh, K. P. and Srivastava, K.: Seasonal variation in the biomass and non-structural carbohydrate content of fine roots of teak (Tectona grandis L. f.) plantations in a dry tropical region, Tree Physiol., 1(1), 31–36, doi:10.1093/treephys/1.1.31, 1986.

Smith, B., Prentice, I. C. and Sykes, M. T.: Representation of vegetation dynamics in the modelling of terrestrial ecosystems: Comparing two contrasting approaches within European climate space, Glob. Ecol. Biogeogr., 10(6), 621–637, doi:10.1046/j.1466-822X.2001.00256.x, 2001.

Smith, M. G., Miller, R. E., Arndt, S. K., Kasel, S., and Bennett, L. T.: Whole-tree distribution and temporal variation of non-structural carbohydrates in broadleaf evergreen trees, Tree

https://doi.org/10.5194/egusphere-2022-835
Preprint. Discussion started: 5 October 2022

Physiol, 38, 570–581, https://doi.org/10.1093/treephys/tpx141, 2018.

Stevens-Rumann, C. S., Kemp, K. B., Higuera, P. E., Harvey, B. J., Rother, M. T., Donato, D. C., Morgan, P. and Veblen, T. T.: Evidence for declining forest resilience to wildfires under climate change, Ecol. Lett., 21(2), 243–252, doi:10.1111/ele.12889, 2018.

Sveinbjörnsson, B., Smith, M., Traustason, T., Ruess, R. W. and Sullivan, P. F.: Variation in carbohydrate source-sink relations of forest and treeline white spruce in southern, interior and northern Alaska, Oecologia, 163(4), 833–843, doi:10.1007/s00442-010-1597-1, 2010.

Tei, S., Sugimoto, A., Liang, M., Yonenobu, H., Matsuura, Y., Osawa, A., Sato, H., Fujinuma, J. and Maximov, T.: Radial Growth and Physiological Response of Coniferous Trees to Arctic Amplification, J. Geophys. Res. Biogeosciences, 122(11), 2786–2803, doi:10.1002/2016JG003745, 2017.

Wang, Z., Zhou, Z. and Wang, C.: Defoliation-induced tree growth declines are jointly limited by carbon source and sink activities, Sci. Total Environ., 762, 143077, doi:10.1016/j.scitotenv.2020.143077, 2021.

Watanabe, S., Hajima, T., Sudo, K. and Nagashima, T.: MIROC-ESM: model description and basic results of CMIP5-20c3m experiments, Geosci. Model Dev. Discuss., 4(2), 1063–1128, doi:10.5194/gmdd-4-1063-2011, 2011.

Weedon, G. P., Balsamo, G., Bellouin, N., Gomes, S., Best, M. J., and Viterbo, P.: The WFDEI Meteorological Forcing Data, Research Data Archive at the National Center for Atmospheric Research, Computational and Information Systems Laboratory, https://doi.org/10.5065/486N-8109, 2018. Accessed 11 Dec 2020.

Woodruff, D. R. and Meinzer, F. C.: Water stress, shoot growth and storage of non-structural carbohydrates along a tree height gradient in a tall conifer, Plant, Cell Environ., 34(11), 1920–1930, doi:10.1111/j.1365-3040.2011.02388.x, 2011.

Würth, M. K. R., Peláez-Riedl, S., Wright, S. J. and Körner, C.: Non-structural carbohydrate pools in a tropical forest, Oecologia, 143(1), 11–24, doi:10.1007/s00442-004-1773-2, 2005.

Xu, C., Liu, H., Anenkhonov, O. A., Korolyuk, A. Y., Sandanov, D. V., Balsanova, L. D.,

https://doi.org/10.5194/egusphere-2022-835
Preprint. Discussion started: 5 October 2022

940 Naidanov, B. B. and Wu, X.: Long-term forest resilience to climate change indicated by
941 mortality, regeneration, and growth in semiarid southern Siberia, Glob. Chang. Biol., 23(6),
942 2370–2382, doi:10.1111/gcb.13582, 2017.
943
944 Zheng, Y., Shen, R., Wang, Y., Li, X., Liu, S., Liang, S., Chen, J. M., Ju, W., Zhang, L. and Yuan,
945 W.: Improved estimate of global gross primary production for reproducing its long-Term
946 variation, 1982-2017, Earth Syst. Sci. Data, 12(4), 2725–2746, doi:10.5194/essd-12-2725-
947 2020, 2020.
948